Supplement of Earth Syst. Sci. Data, 16, 15–34, 2024
https://doi.org/10.5194/essd-16-15-2024-supplement

Open Access Earth System Science Data

Supplement of

Sensor-independent LAI/FPAR CDR: reconstructing a global sensor-independent climate data record of MODIS and VIIRS LAI/FPAR from 2000 to 2022

Jiabin Pu et al.

Correspondence to: Kai Yan (kaiyan@bnu.edu.cn)

Supplementary.

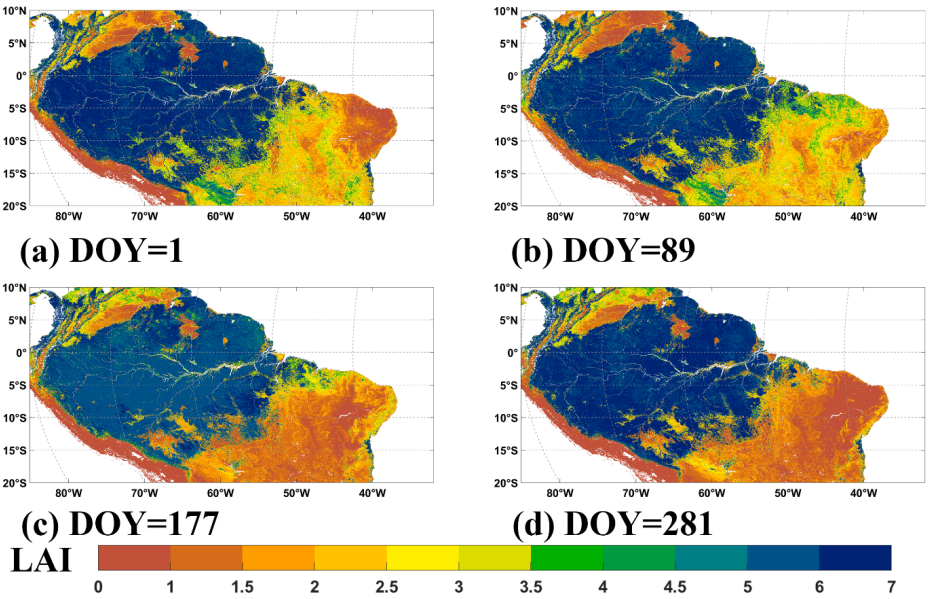

Figure S1. The spatial performance of the LAI reference for DOY 1 (a), 89 (b), 177 (c), 281 (d) in the Amazon Forest region.

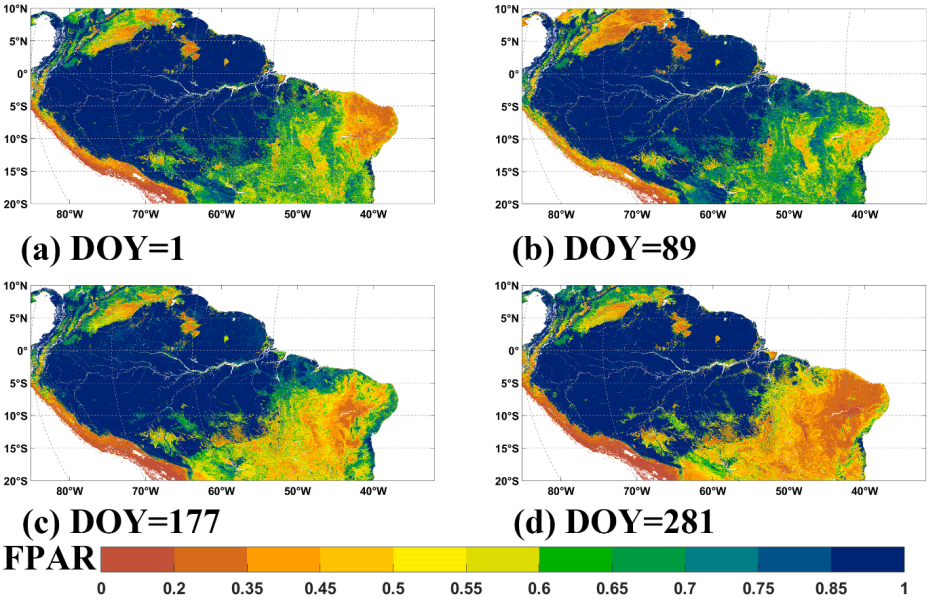

Figure S2. Same as Fig. S1 but for FPAR. The spatial performance of the FPAR reference for DOY 1 (a), 89 (b), 177 (c), 281 (d) in the Amazon Forest region.

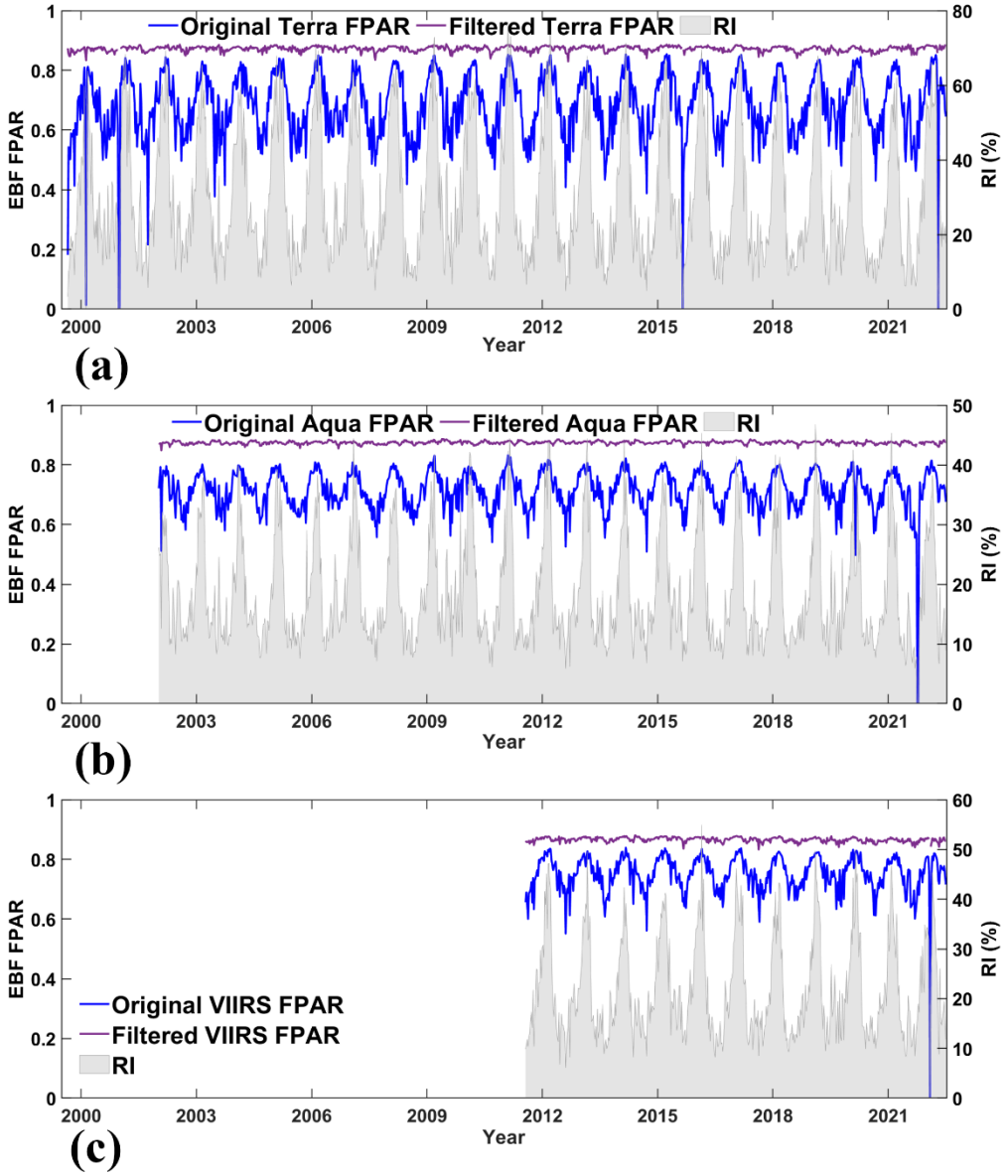

Figure S3. Same as Fig. 3 but for FPAR. The temporal comparisons between the original Terra/Aqua/VIIRS FPAR and Filtered Terra/Aqua/VIIRS FPAR for the EBF of Amazon Forest region.

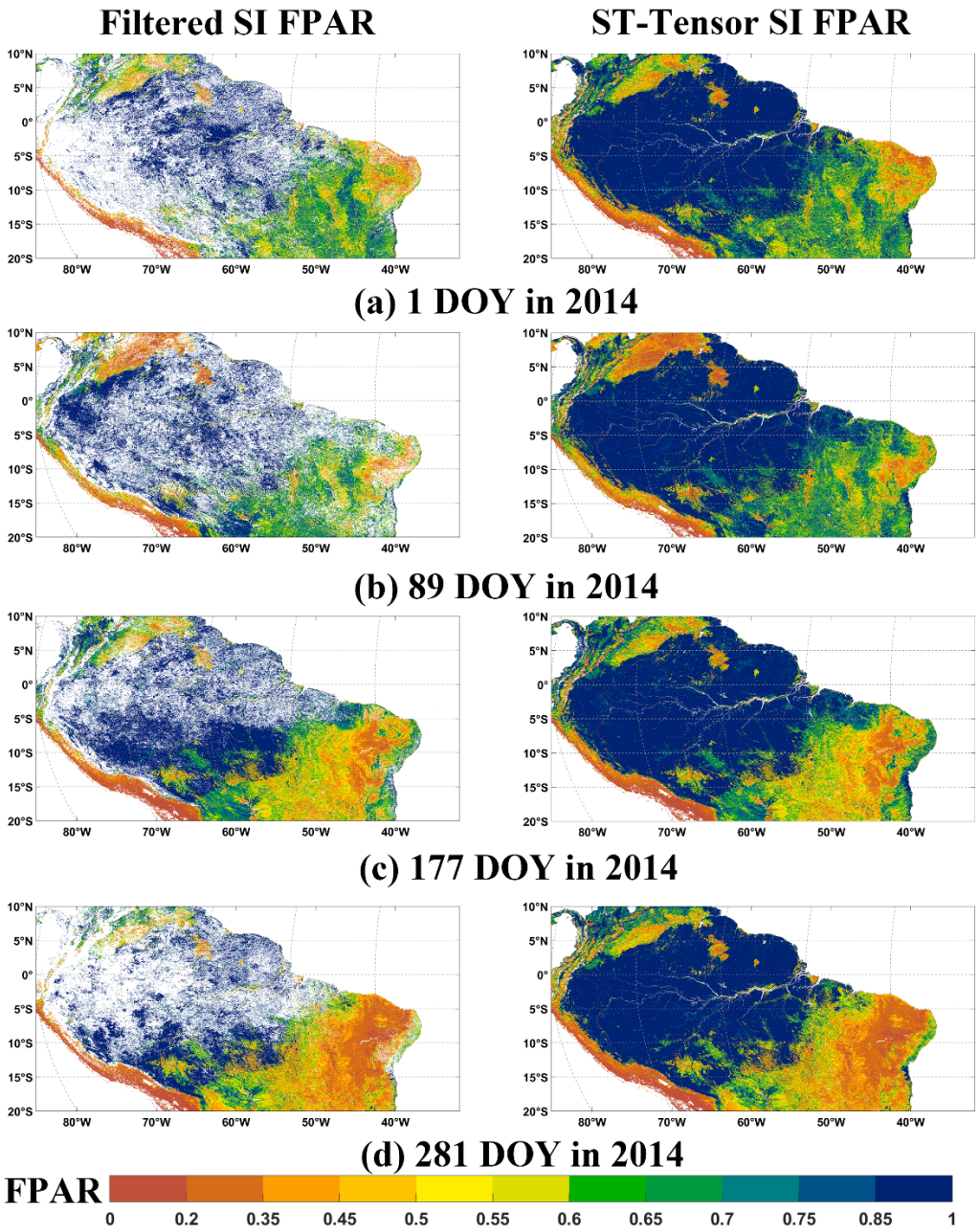

Figure S4. Same as Fig. 6 but for FPAR. The spatial performance of the ST-Tensor method for DOY 1 (a), 89 (b), 177 (c), 281 (d) in 2014 year in the Amazon Forest region.

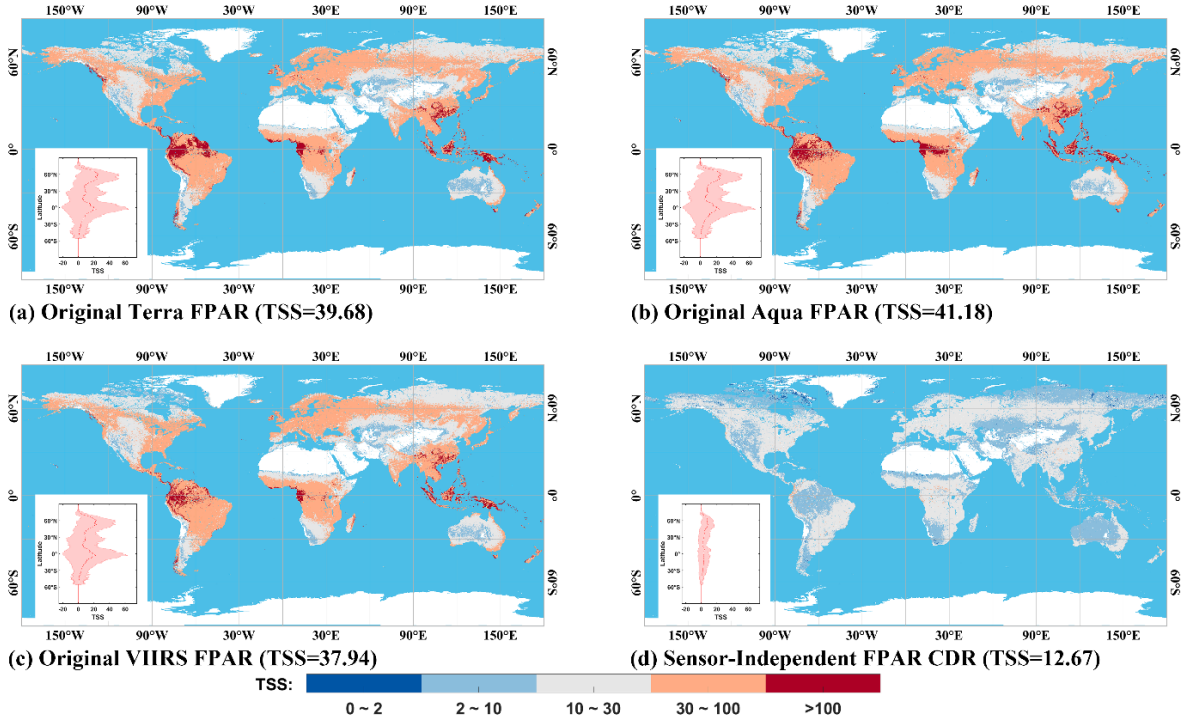

15 **Figure S5.** Same as Fig. 7 but for FPAR. The global distribution of FPAR TSS in each 0.05 degree× 0.05 degree grid from 2013 to 2022.

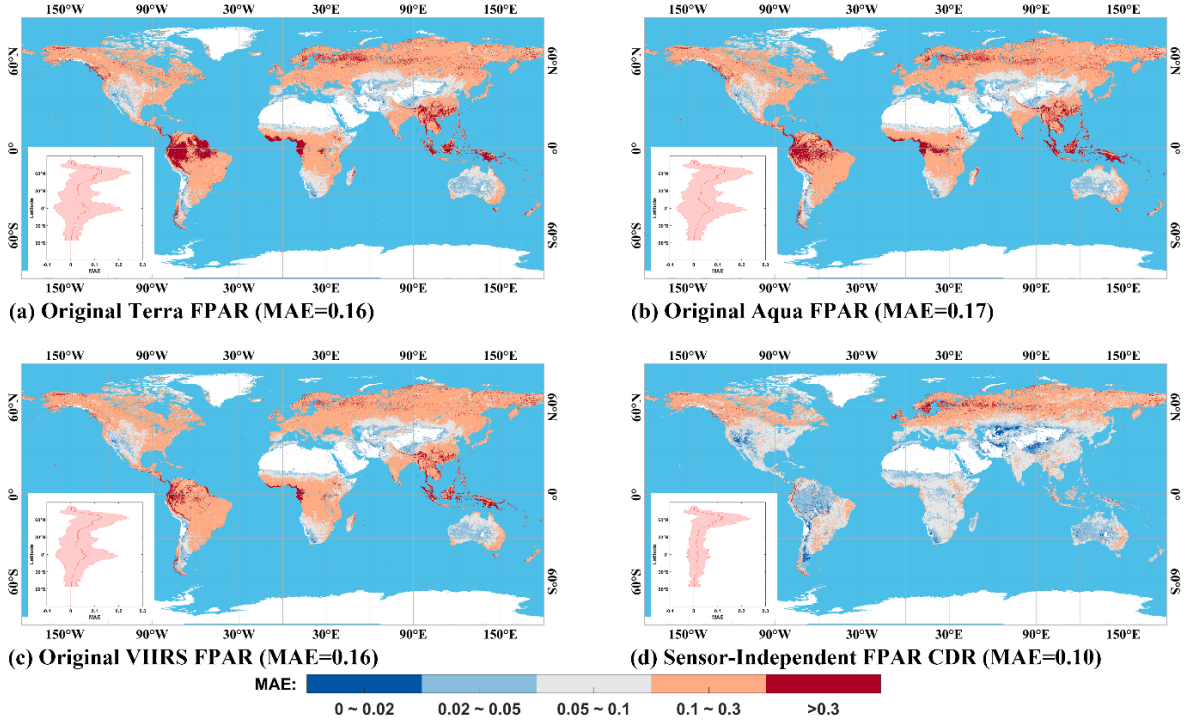

Figure S6. Same as Fig. 8 but for FPAR. The global distribution of FPAR MAE in each 0.05 degree× 0.05 degree grid from 2013 to 2022.

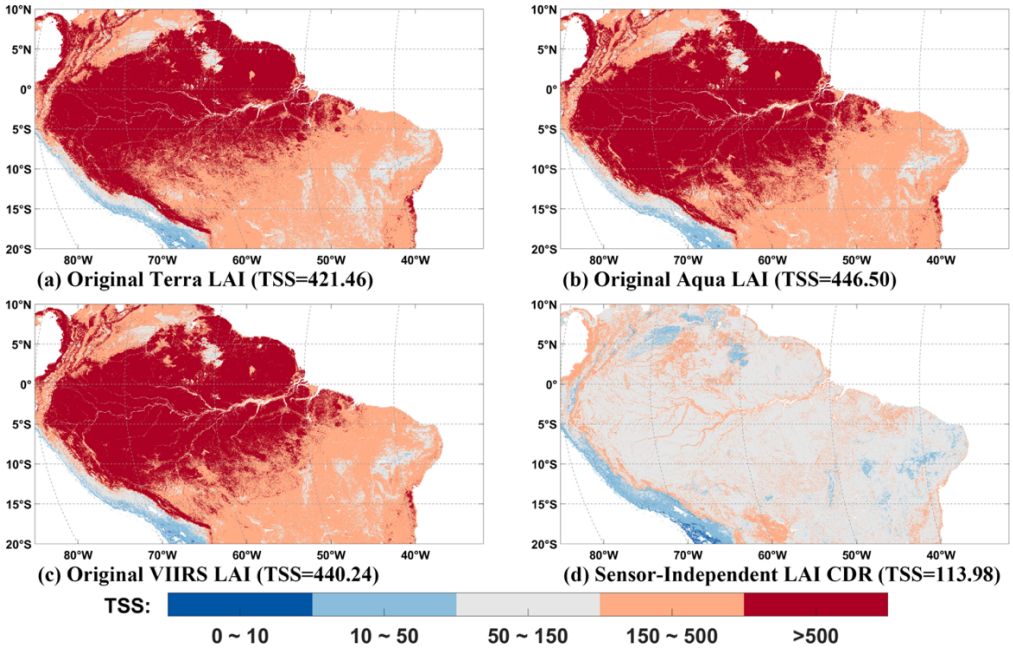

Figure S7. Same as Fig. 7 but for the Amazon Forest region. The spatial distribution of LAI TSS in each 500m × 500m grid, with sinusoidal projection over the selected Amazon Forest region (zoom-in case in Fig. 1), from 2013 to 2022.

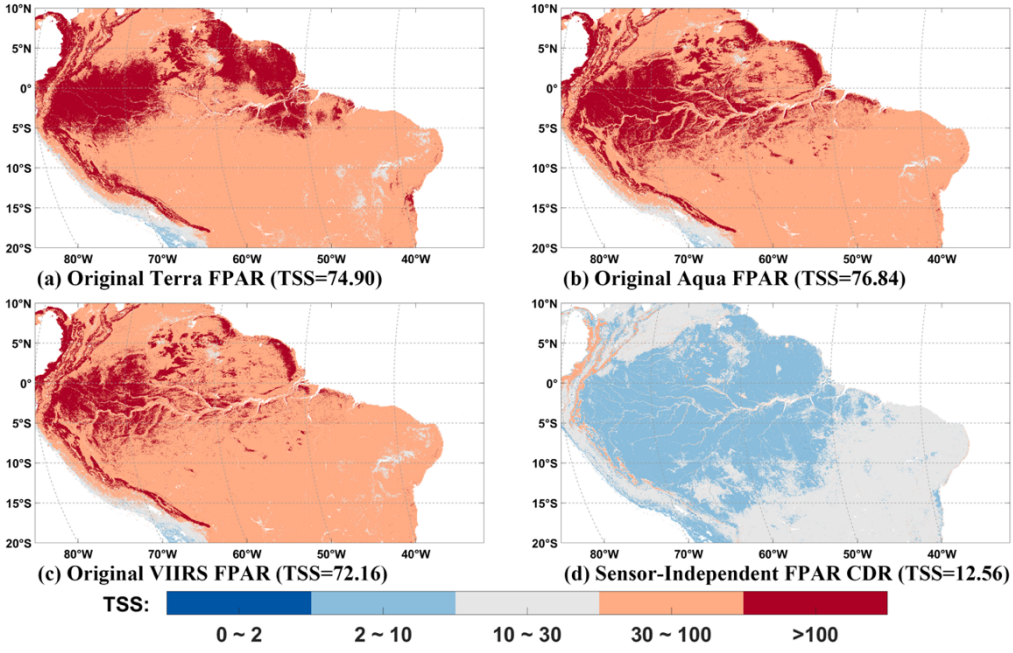

Figure S8. Same as Fig. S7 but for FPAR. The spatial distribution of FPAR TSS in each 500m × 500m grid, with sinusoidal projection over the selected Amazon Forest region (zoom-in case in Fig. 1), from 2013 to 2022.

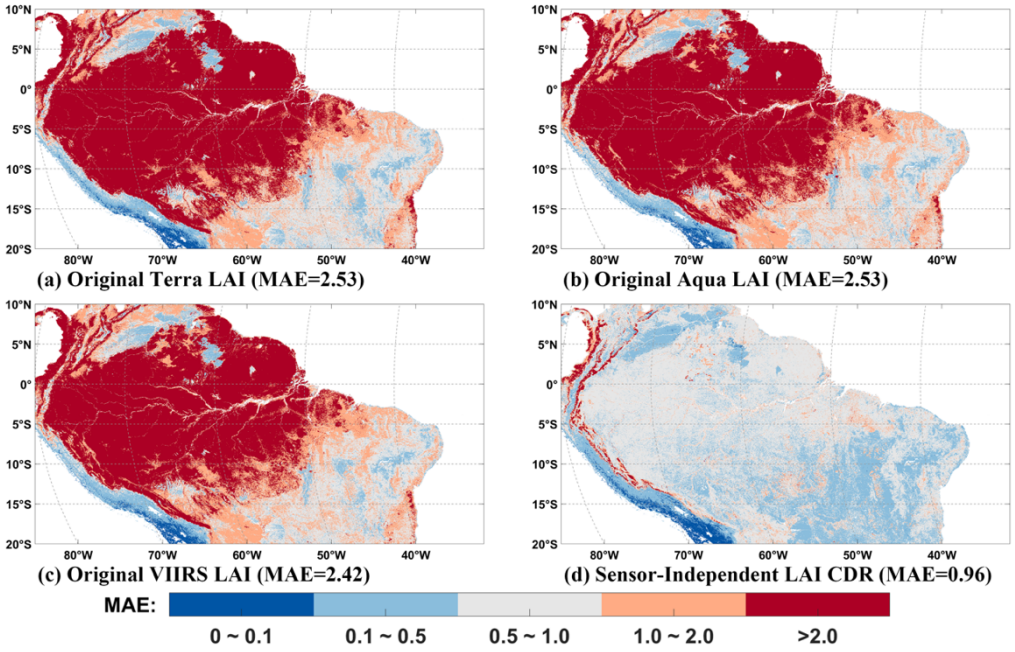

Figure S9. Same as Fig. S7 but the metric is MAE. The spatial distribution of LAI MAE in each 500m × 500m grid, with sinusoidal projection over the selected Amazon Forest region (zoom-in case in Fig. 1), from 2013 to 2022.

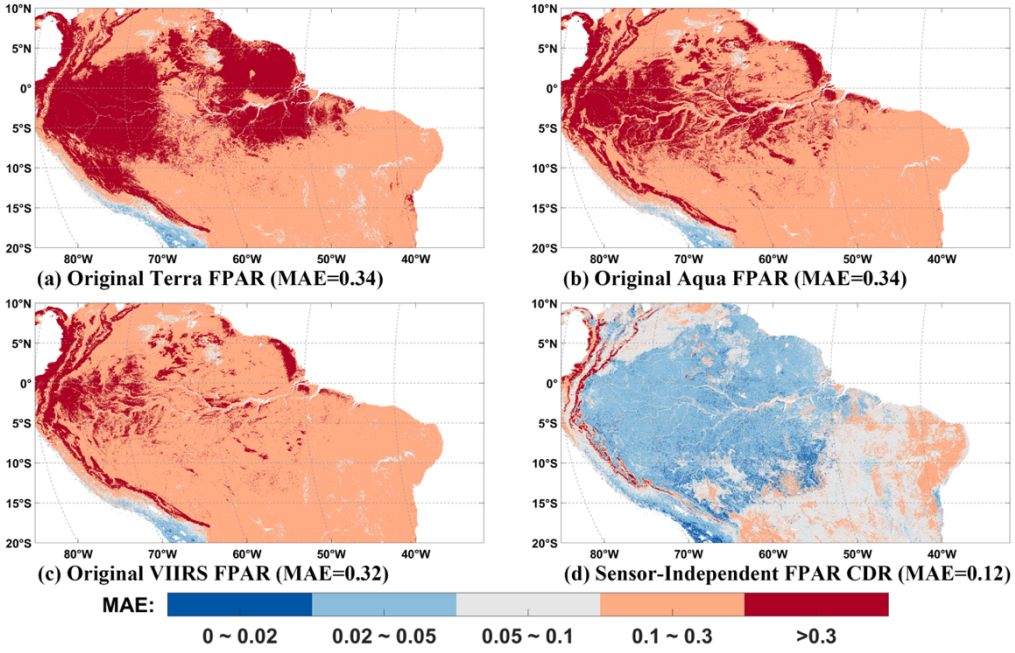

Figure S10. Same as Fig. S9 but for FPAR. The spatial distribution of FPAR MAE in each 500m × 500m grid, with sinusoidal projection over the selected Amazon Forest region (zoom-in case in Fig. 1), from 2013 to 2022.

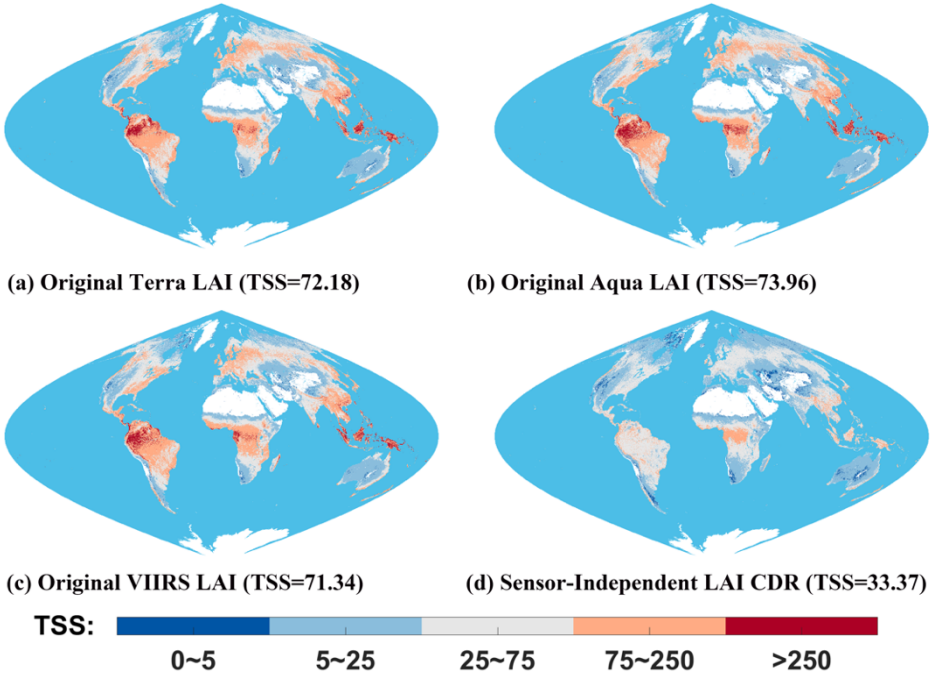

Figure S11. Same as Fig. S7 and the spatial resolution is 5km and the temporal resolution is bimonthly. The global distribution of LAI TSS in each 5km× 5km grid, with sinusoidal projection, from 2013 to 2022.

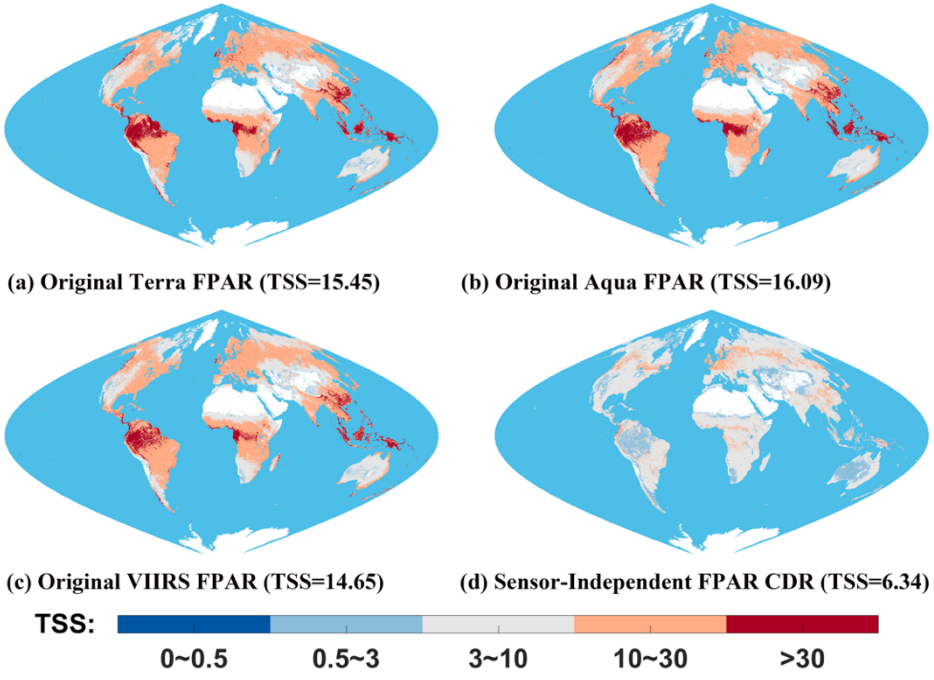

Figure S12. Same as Fig. S11 but for FPAR. The global distribution of FPAR TSS in each 5km× 5km grid, with sinusoidal projection, from 2013 to 2022.

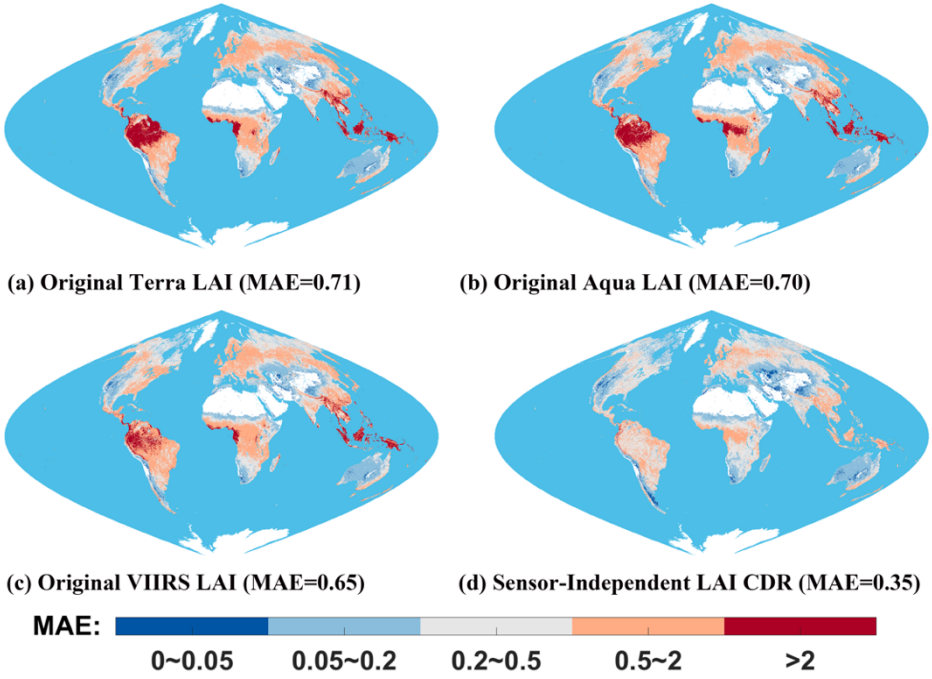

Figure S13. Same as Fig. S11 but the metric is MAE. The global distribution of LAI MAE in each 5km× 5km grid, with sinusoidal projection, from 2013 to 2022.

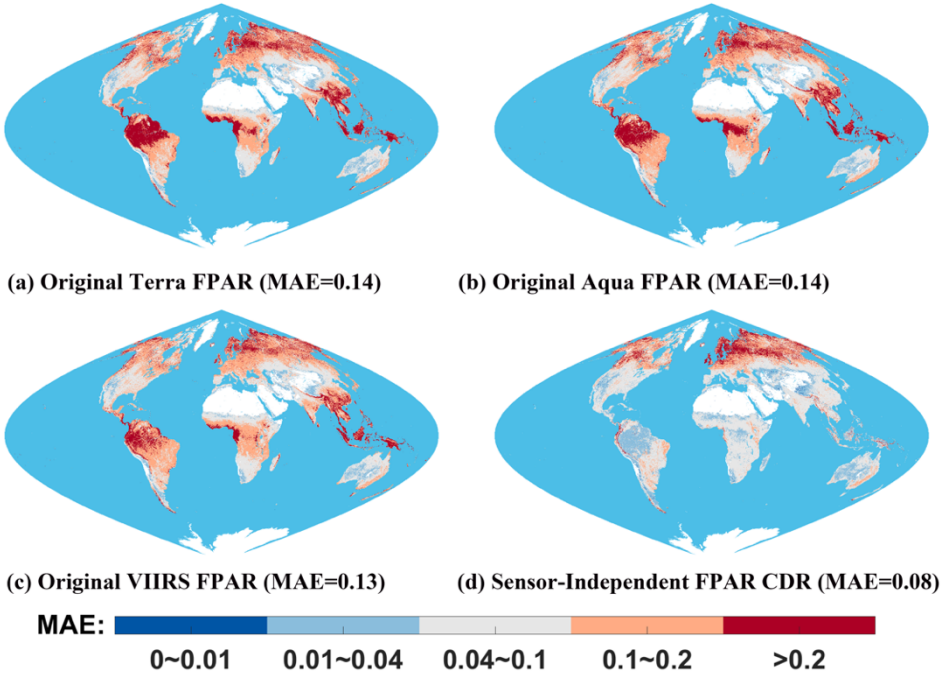

Figure S14. Same as Fig. S13 but for FPAR. The global distribution of FPAR MAE in each 5km× 5km grid, with sinusoidal projection, from 2013 to 2022.

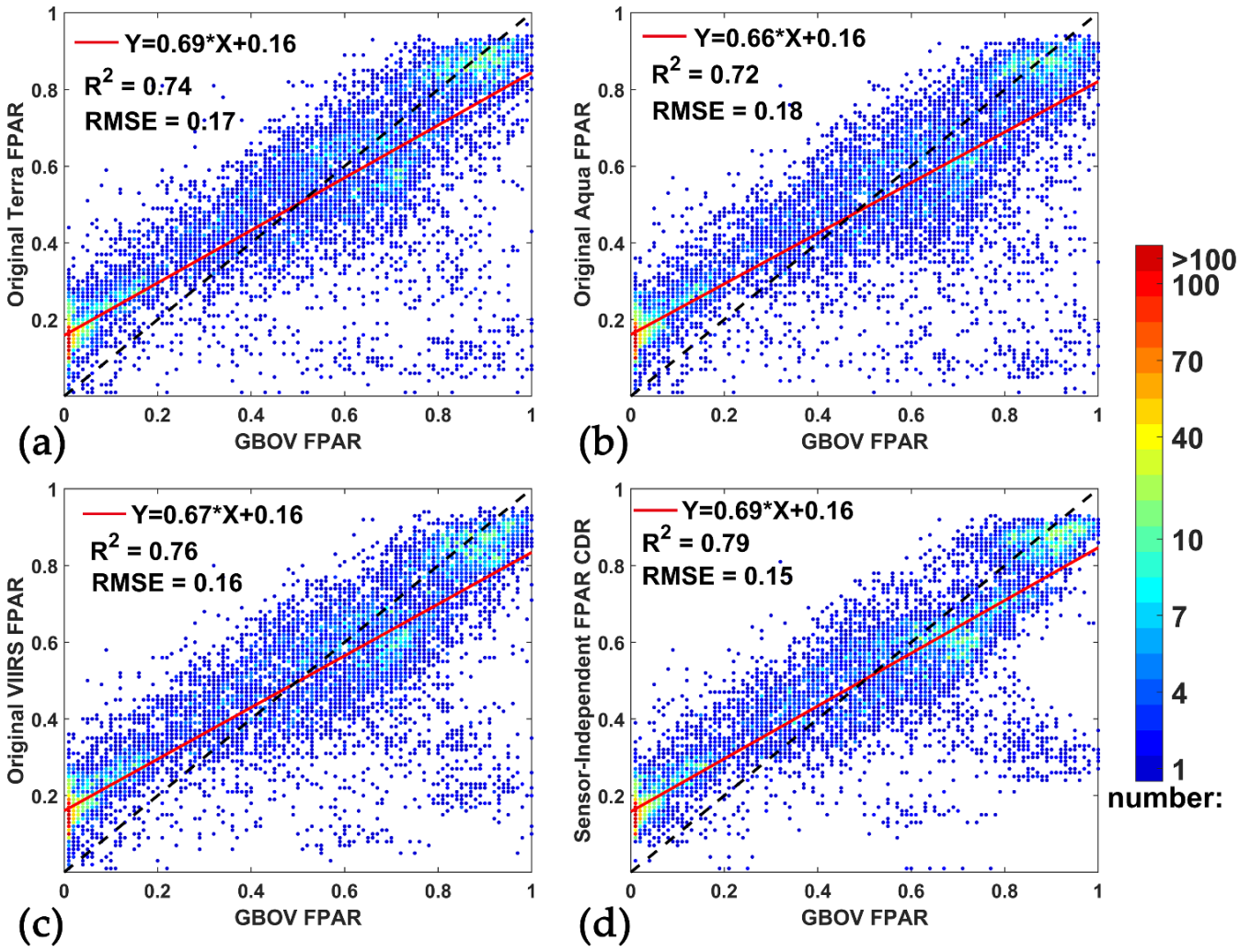

Figure S15. Same as Fig. 9 but for FPAR. Comparisons of original Terra/Aqua/VIIRS FPAR and SI FPAR CDR with ground GBOV FPAR.

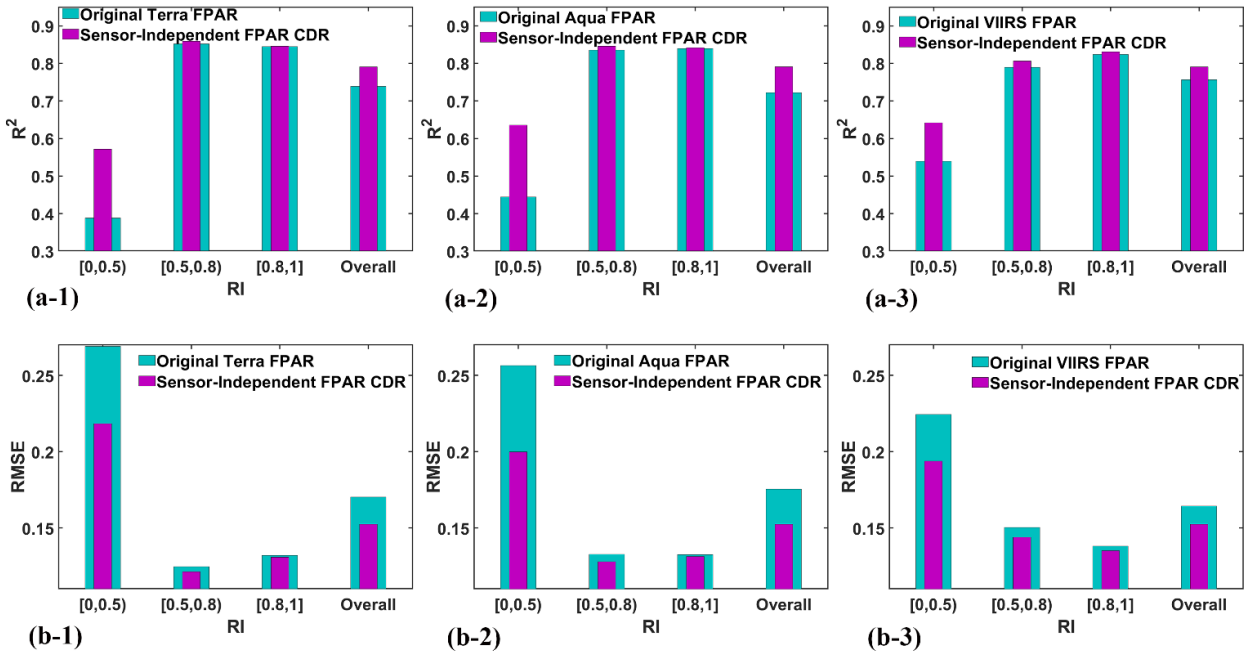

45 **Figure S16.** Same as Fig. 10 but for FPAR. The $\mathbf{R^2}$ and RMSE between original Terra/Aqua/VIIRS FPAR and SI FPAR CDR and GBOV FPAR in different RI ranges.

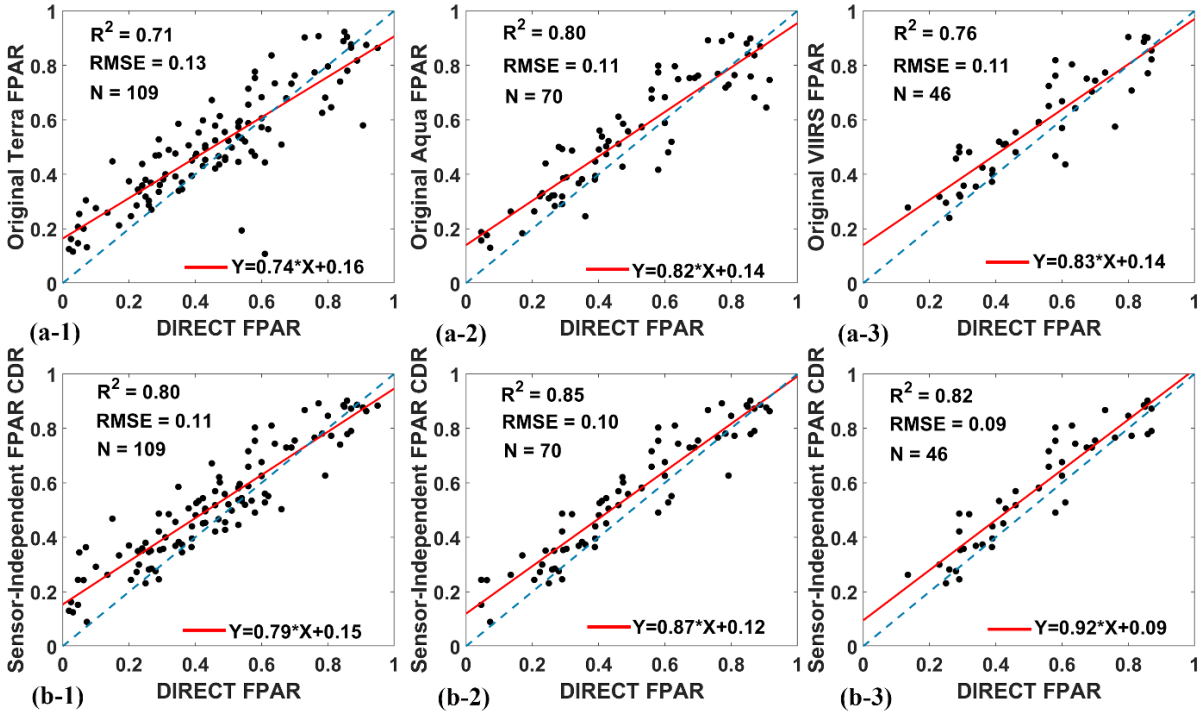

Figure S17. Same as Fig. 11 but for FPAR. Comparisons of original Terra/Aqua/VIIRS FPAR and SI FPAR CDR with ground DIRECT2.1 FPAR measurements.